



Cite this: *Mater. Adv.*, 2020, **1**, 2068

Effect of high energy proton irradiation on MAPbI₃ films for space applications observed by micro-Raman spectroscopy†

Walter O. Herrera Martínez,^{ab} Paula Giudici,^{ab} Natalia B. Correa Guerrero,^{ab} M. Luján Ibarra^a and M. Dolores Perez^{ID, *ab}

Irradiation of samples with 10 MeV protons is a standard test for simulation of the outer space environment in order to qualify devices and materials for space applications. Micro-Raman spectroscopy allows one to determine the irradiation effect on methylammonium lead iodide (MAPbI₃) thin films under ambient conditions and encapsulated. For the unprotected films, the vibrational modes matched previously reported lead oxide phonon frequencies and the appearance of superficial oxides was confirmed by EDAXS analysis. However, the Raman shifts corresponding to PbO were not observed for the irradiated encapsulated samples, indicating that oxidation occurs after surface exposure to ambient oxygen. Similar effects have been observed by photooxidation where the highly reactive superoxide radical is involved in the oxidation mechanism. We propose that irradiation promotes excitation of the electron cloud, which readily reduces the surface adsorbed oxygen, and this later bonds to the accessible Pb atoms.

Received 7th August 2020,
Accepted 13th August 2020

DOI: 10.1039/d0ma00583e

rsc.li/materials-advances

1 Introduction

The characteristic optoelectronic properties, potential low cost and the ease of fabrication make lead halide perovskites a promising material for a wide range of electronic applications, like humidity sensors,¹ lasers,^{2,3} 3D arrays for image sensors,⁴ and solar cells.^{5,6} In particular, the use of lead halide perovskites in photovoltaic devices has received a large amount of attention due to the high conversion efficiencies achieved in only a few years. Different properties of perovskite films have been studied at length, which include thermodynamic properties,⁷ the effects of solvent processing,⁸ degradation mechanisms,⁹ and ionic diffusion,¹⁰ just to name a few. These efforts have helped to understand the characteristics of this novel material, allowing researchers to fabricate perovskite solar cells with power conversion efficiencies of up to 25%.¹¹

Outer space is a hostile environment for semiconductor materials; for many years researchers have studied radiation damage of Si photovoltaics and, most recently, of III-V solar cells for space applications, in order to understand the deterioration of the electronic properties and defect formation.^{12,13}

Hybrid metal halide perovskite materials present properties, like high optical density, long carrier diffusion length,^{14,15} small carrier recombination times and a high tolerance to defects,⁵ that make them ideal candidates for solar cells and particularly interesting for space applications.¹⁶ While radiation can cause defects in typical semiconductors used in solar cells, generating losses in J_{sc} (short-circuit current) and V_{oc} (open-circuit voltage), lead halide perovskite solar cells are not strongly affected by 50 keV protons as shown by Miyazawa *et al.*¹⁷ Even for high energy proton irradiation of 68 MeV and fluence higher than 10^{12} p cm⁻², perovskite solar cells have been shown to exhibit negligible performance degradation.¹⁸

While lead halide perovskites are hybrid crystalline materials with interesting chemical and physical properties, they are also very sensitive to moisture, light and moderate temperatures, and so their characterization must be performed carefully in order to not modify the synthesized structures. Micro-Raman spectroscopy has proven to be a powerful technique to determine defects in different materials like SiC,^{19,20} III-V semiconductors (like InAs and GaAs),²¹ graphene²² and two dimensional semimetals.²³ Some Raman studies on lead halide perovskites have been carried out recently that have allowed the analysis of organic-inorganic interactions and their crystalline phases.²⁴⁻²⁷ These studies have shown many effects, like structural changes correlated with local moisture that induce degradation of the film,²⁶ torsional vibrations related to different degrees of order in material domains, gradual spectral changes associated with new photoinduced structure possibly caused by

^a Departamento Energía Solar, GlyA, Centro Atómico Constituyentes, CNEA, Av. Gral. Paz 1499, (1650) San Martín, Buenos Aires, Argentina.

E-mail: mdperez@tandar.cnea.gov.ar

^b Instituto de Nanociencia y Nanotecnología, CNEA-CONICET, Av. Gral. Paz 1499, (1650) San Martín, Buenos Aires, Argentina

† Electronic supplementary information (ESI) available. See DOI: 10.1039/d0ma00583e



rearrangement of the inorganic Pb-I scaffold or structural response to ion motion.²⁸

In this work we report the characterization by micro-Raman spectroscopy of $\text{CH}_3\text{NH}_3\text{PbI}_3$ (methylammonium lead iodide, MAPbI_3) thin films after sample irradiation with 10 MeV protons and $10^{11} \text{ p cm}^{-2}$ fluence. The irradiation conditions are typically used to simulate irradiation inside the inner Van Allen belt in low-earth orbit (LEO). LEO is the most commonly used orbit for most satellites except for communication satellites that move in geostationary orbit.¹³ We report the vibrational modes of films under exposure to radiation while being careful not to produce degradation by the Raman laser intensity and demonstrate the inherent material resistance to permanent irradiation defect formation.

2 Experimental method

Glass substrates were cleaned with aqueous detergent solution under ultrasound for 10 min and later successively submerged in acetone and a 1:1 mixture of ethanol and isopropyl alcohol for further washing. The substrates were later dried under a nitrogen (99.998%) flow and finally cleaned with microwave plasma.

Highly crystalline perovskite thin films of $\sim 320 \text{ nm}$ measured by SEM were obtained by a one-step method, according to the previously reported recipe using $\text{PbI}_2 : \text{CH}_3\text{NH}_3\text{I} : \text{DMSO}$ in a 1:1:1 stoichiometric relation.²⁹ Briefly, lead iodide (99.995%, Beantown Chemical) was completely dissolved in a solution mixture of dimethyl sulfoxide (DMSO) and dimethylformamide (DMF) (Merck), and heated at 70–80 °C. $\text{CH}_3\text{NH}_3\text{I}$ (methylammonium iodide, MAI) (>99%, Greatcell Solar) was added to the resulting solution after cooling. The solution was then filtered through a PVDF syringe filter (0.45 μm pores) and spin-coated onto a glass substrate at 4000 rpm for 50 seconds. Chlorobenzene was added during spin coating as an antisolvent to enhance the crystallinity. Encapsulation by PMMA was done by spin-coating (10 mg mL^{-1}) the solution onto the perovskite films at 4000 rpm for 30 s.

The radiation exposure of the samples was performed using a tandem type accelerator at CNEA (Tandar). The radiation beam consisted of 10 MeV proton energy and $1 \times 10^{11} \text{ p cm}^{-2}$ fluence. The beam intensity was calibrated using an array of Faraday cups at the back-end of the irradiation chamber. The calibration Faraday cup current was measured with a Keithley 6514 electrometer. The perovskite films, both encapsulated and not encapsulated, are introduced into the irradiation chamber with half of the surface film exposed and the other half protected from radiation with thick glass, in order to have a control MAPbI_3 film that has undergone the same experimental conditions but has not suffered irradiation.

The Raman characterization was performed in backscattering configuration with a LabRAM HR UV-vis-NIR-Horiba Jobin Yvon spectrometer with a 2.5 cm^{-1} spectral resolution. The setup was equipped with two excitation sources of 514 nm (Ar^+ laser) and 633 nm (He-Ne laser). The Raman spectra were recorded with an integration time of 60 s using a $50\times$ objective (3 μm spot on the sample) and a laser power between 0.03 and 1 mW.

Field Emission-Scanning Electron Microscopy (FE-SEM) images were obtained with a ZEISS LEO 982 GEMINI field emission electron microscope in secondary electron mode, using an in-lens detector to improve the resolution (CMA, Facultad de Ciencias Exactas y Naturales, UBA). X-ray diffraction measurements were performed using Empyrean PANanalytical equipment with a $\text{Cu K}\alpha$ monochromatic radiation source and PIXcel 3D ultrafast detector, scanning from 10° to 60° (2θ) in 0.02 steps.

3 Results and discussion

Highly crystalline MAPbI_3 perovskite thin films were prepared and selectively irradiated under simulated space radiation conditions for a typical LEO mission. The topography of both films was observed by scanning electron microscopy, SEM. Fig. 1 shows both the irradiated and non-irradiated surfaces for different magnifications. An extent of surface reconstruction with shrinking grains that conglomerate in certain areas can be observed for the MAPbI_3 surface after irradiation. The close-up images reveal that after irradiation some grains remain with similar size and shape ($\sim 100 \text{ nm}$) but others seem to break up into many smaller ones with different crystalline order and grouped in specific regions.

The Raman spectra of the perovskite MAPbI_3 films were obtained for both the irradiated and non-irradiated materials. The Raman shifts are significantly different for both films, as can be observed in Fig. 2. Both spectra were obtained using a very low intensity laser ($P < 25 \text{ W cm}^{-2}$) in order to minimize degradation effects due to the local heating by the Raman laser.^{26,28,30}

The as-prepared film measured under environmental conditions shows a Raman spectrum that is similar to the previously reported literature.³⁰ Contrarily, the irradiated film shows bands at 143 , 284 and 337 cm^{-1} that have not been reported previously for MAPbI_3 films with low power density measurements.²⁶ The Raman shifts obtained for the irradiated samples are, however, very similar to previously reported PbO films. The band at 143 cm^{-1} can be assigned to the A_{1g} vibrational mode, resulting from the motion of the lead atoms parallel to the c -axis in a PbO structure.³¹ PbO formation could account for the surface grain reconstruction observed in the SEM images. It is unfathomable that the oxide may be caused exclusively by proton irradiation since there is no oxygen atom within the MAPbI_3 chemical formula. Evidently, it cannot simply be an irradiation defect but it must be coupled to exposure of the irradiated material to an oxygen source.

The formation of PbO from methylammonium lead iodide films has been described in recent work in degradation induced by light.^{32,33} In particular, the reports that suggest the mechanisms of oxide formation by means of extensive first-principles calculations propose that excess photogenerated electrons in MAPbI_3 react with ambient molecular O_2 to create the highly reactive superoxide ion (O_2^-). As opposed to molecular oxygen, the superoxide ion has a relatively higher bonding



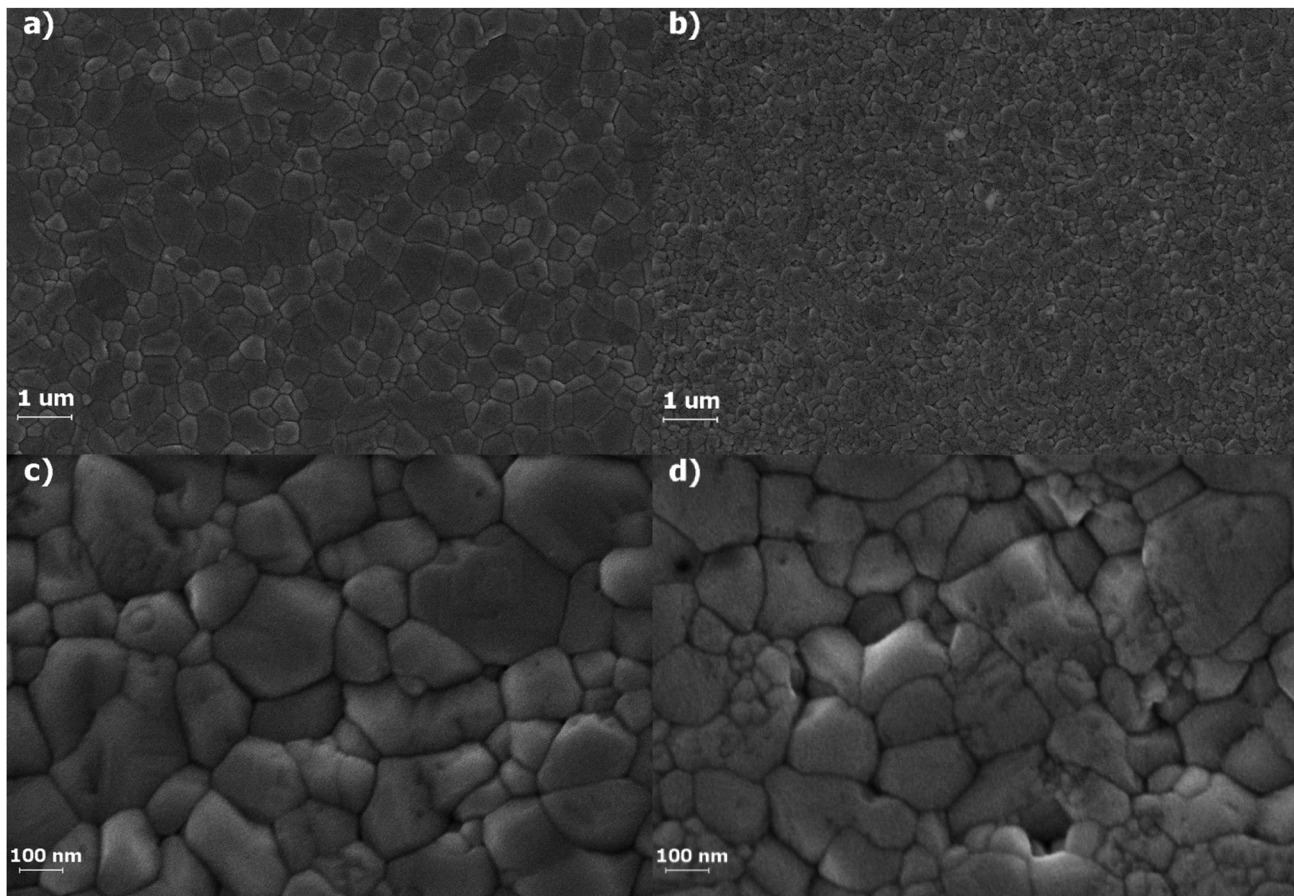
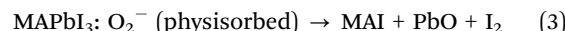
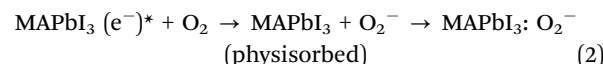
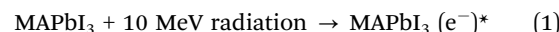


Fig. 1 SEM images for MAPbI_3 films as-prepared (a and c) and after irradiation (b and d).

energy to the MAPbI_3 surface, both to the Pb–I terminated and the MAI terminated (001) surfaces. Ouyang *et al.* and Zhang *et al.* suggest that physisorption is rapidly followed by chemisorption, whereas the physisorbed O_2 will not form a chemical bond.^{34,35} Chemisorption by formation of a Pb–O bond occurs either by replacing an iodine atom that volatizes as I_2 , or by displacing two hydrogen atoms from the methylammonium that consequently form H_2O leaving behind the Pb–O bond. In this work, under normal experimental conditions, we do not observe PbO formation by photodegradation since the

non-irradiated sample (that underwent the same experimental conditions as the irradiated sample) presents a Raman spectrum corresponding to neat perovskite samples as reported previously. Contrarily, the proton irradiated samples show extensive lead oxide formation. In this case, we propose that the superoxide ion is formed by the interaction of excess electrons promoted in the perovskite film by the 10 MeV proton radiation. At this energy, protons are 10^5 times more likely to interact with the electron cloud than with the structural nucleus, thus causing a density of high energy and highly reactive electrons. The resulting highly reactive surface reduces atmospheric oxygen to form superoxide ions that later physisorb and chemisorb to the perovskite surface. The proposed reaction mechanism is as follows:



It is not clear whether oxygen incorporation occurs inside the irradiation chamber or after the sample is extracted and exposed to ambient air. Even though the oxygen concentration

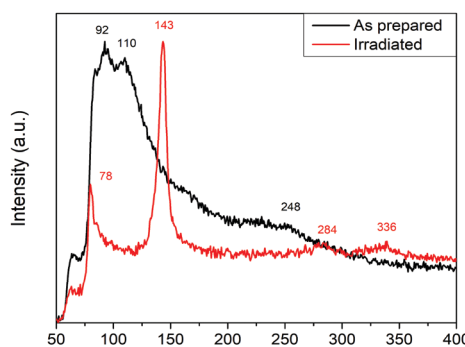


Fig. 2 Raman spectra of irradiated (red) and non-irradiated (black) MAPbI_3 thin films.



in a vacuum chamber is very low, it could be enough to react with the highly reactive excess electrons on the MAPbI_3 surface.

Superoxide formation must occur faster than the MAPbI_3 (e^-)^{*} decay rate to the ground state. Further studies to evaluate the lifetime of the perovskite excited state after irradiation should be carried out by time resolved experiments coupled to the particle accelerator experimental line in order to determine the relevance of the oxygen concentration to the mechanism second step. However, we believe it is unlikely that the MAPbI_3 (e^-)^{*} state would live long enough before the chamber can be opened safely after irradiation (2–3 hours).

The Raman spectrogram for PbO films has been thoroughly studied in previous work by Wiechert *et al.*³¹ In that report, the α - and β - PbO polymorphs present specific intensity ratios for the 284 and 335 nm signal. For ratios $I(284)/I(335) > 1$, the predominant phase is the orthorrombic β - PbO phase, while the α -phase is predominant when the ratio is inverted. Both the tetragonal α - PbO and the orthorrombic β - PbO phases can be observed for the irradiated samples in different regions of the sample, with ratios varying from 1.46 to 0.84 for Fig. 3, top and bottom, respectively.

A simple method to confirm that the PbO polymorph formation is originated by the convolution of the proton irradiation and later exposure to atmospheric oxygen is by encapsulating the surface with PMMA. PMMA is transparent to radiation due to the very small thickness and it efficiently protects the surface from atmospheric oxygen. Fig. 4 shows the Raman spectra for both irradiated MAPbI_3 samples with and without PMMA encapsulation. The unprotected surface shows the typical PbO Raman shift at 140 cm^{-1} as observed in Fig. 2. Contrarily, the encapsulated sample does not present significant oxidation into PbO as the Raman spectra do not present the corresponding PbO shifts. We propose that the excited electron cloud caused by irradiation will recombine and reversibly relax to the ground state if no oxidative compound meets the interface. It must be mentioned that the Raman spectrum for the encapsulated sample does not exactly match the neat perovskite spectra presented in Fig. 2 but instead it is similar to

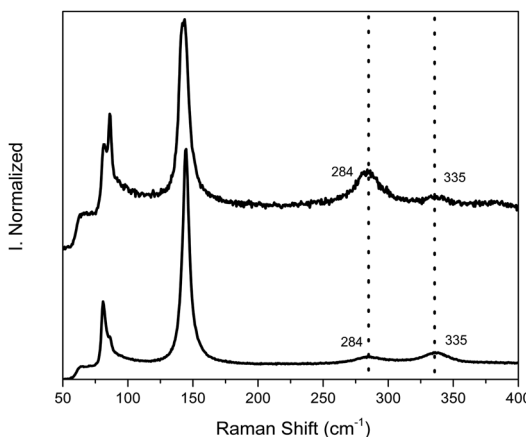


Fig. 3 Raman spectra for irradiated MAPbI_3 films in different regions of the film sample.

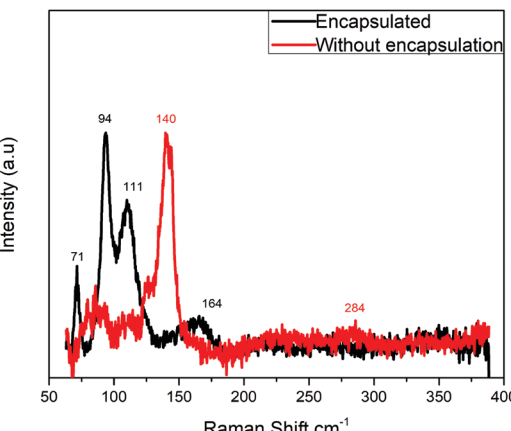


Fig. 4 Raman spectra of irradiated MAPbI_3 thin films encapsulated with PMMA and without encapsulation.

the spectrum of barely degraded perovskite film by Raman laser local heating.^{26,30} The presence of the PMMA top layer demands to use a more intense laser in order to achieve a significant signal. If extremely low power is used, no signal is observed, and therefore we increased the power intensity during the measurement until a good enough signal-to-noise ratio was achieved, causing some perovskite degradation by the Raman laser as reported elsewhere in the literature.^{26,28} The Raman degradation spectra for our perovskite films were measured and presented in the ESI;† no PbO shifts are observed when the film is degraded by the Raman laser with time or by increasing the laser intensity. It can be positively affirmed that proton irradiation does not provoke any permanent defects in the perovskite semiconductor material as opposed to other inorganic semiconductors applied to solar cells like Si, CIGS, III–V, *etc.* This result is in agreement with published literature demonstrating the radiation hardness of perovskite solar cells,^{17,18} where the electronic excitation by irradiation may not provoke oxidation of the adjacent layers (TiO_2 and spiro-OMeTAD, typically) and the film quickly relaxes to its ground state.

The presence of the different atomic elements in the film was evaluated by EDAXS. Table 1 shows the representative sample elements and the percentual difference between the non-irradiated and the irradiated sample, unencapsulated. We observe a clear reduction of the atomic % of Pb and I due to an increase of the O percent for the irradiated samples *vs.* the as-prepared films. Additionally, the MAPbI_3 stoichiometric 3 : 1 iodine to lead ratio is observed, suggesting that the perovskite

Table 1 Atomic percent of representative elements for the irradiated and non-irradiated samples as observed by EDAXS

Element	Non-irradiated MAPbI_3	Irradiated MAPbI_3	% Difference
	Atomic %	Atomic %	
O	19.36	22.48	+16.12
Si	14.64	14.97	+2.25
I	5.96	5.30	-11.07
Pb	1.94	1.76	-9.28



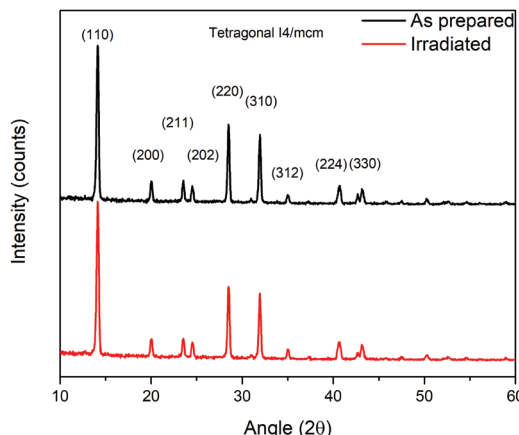


Fig. 5 Grazing angle X-ray diffraction patterns for the fresh and irradiated perovskite film.

crystal still remains as the majority material. A silicon signal is also present as it is part of the glass substrate material (SiO_2). It could be argued that an increase of the oxygen signal would correspond to substrate exposure upon irradiation by formation of holes and craters; however, the Si amount is almost constant for both samples while the oxygen increase is significant for the irradiated samples. The SEM images presented in Fig. 1 also show no apparent substrate exposure.

Further evaluation of the irradiated material was observed by XRD and photoluminescence spectroscopy (PL). The grazing angle X-ray diffraction pattern does not show an appreciable difference for both irradiated and non-irradiated films. The diffractograms are presented in Fig. 5 and show the typical tetragonal MAPbI_3 phase. There are no observable PbI_2 or PbO features from degradation/oxidation either by humidity or by irradiation. The PL emission signal of the MAPbI_3 film also remains mostly unaffected after irradiation (see the ESI†).

The absence of a PbO signal in the X-ray diffraction pattern for the irradiated sample seems to confirm that the bulk perovskite remains unaffected and PbO is only formed as a thin top surface layer that cannot be detected by the DRX technique. As the superoxide reacts with the surface perovskite, it forms a coating film that prevents further reaction from happening as the O_2^- ions can no longer access the deeper MAPbI_3 layer. This passivation effect has been reported earlier for the photodegradation mechanism³⁴ and it is then plausible that in our experiment only a thin top layer of PbO is obtained. During the Raman measurement, the top PbO film may likely absorb the normal incident laser beam, shielding not only the laser from reaching the bottom bulk perovskite but also preventing its weak signal response from being observed.

4 Conclusions

Hybrid organo-lead halide perovskite solar cells reportedly show excellent properties under irradiation for space applications. We investigated the effect of proton irradiation on MAPbI_3 films by Raman measurements and confirmed the perovskite hardness to radiation. The irradiated samples do

not present any new signal in the Raman spectra that could be assigned to a non-reversible chemical change or defect formation. Conversely, when the films are exposed to an ambient atmosphere after irradiation, the Raman signal reveals the formation of PbO . The incorporation of oxygen into the perovskite structure is assumed to follow the same mechanism as photooxidation: the excited electron cloud caused by collisions of high energy protons promotes superoxide formation, which readily oxidizes the MAPbI_3 top surface into PbO . The oxide formation results in a thin top layer that passivates the bulk perovskite and prevents further oxidation. The presence of superficial oxide on the irradiated film exposed to an ambient atmosphere was confirmed by EDAXS, whereas the GI-XRD measurement does not reveal any PbO signal, and only the crystallographic planes from the neat perovskite can be observed. These observations are consistent with the presence of a top thin PbO layer: a very weak Raman signal from the perovskite (screened by the PbO layer), a strong PbO Raman signal and an X-ray diffractogram showing only the bulk halide perovskite. We can further conclude that the MAPbI_3 material is inert to high energy proton irradiation as long as it does not come in contact with an oxidizing substance; this is relevant in terms of designing the device architecture when it is subjected to irradiation so that the perovskite layer is not only isolated from atmospheric oxygen but is also in contact with layers that will not promote an oxidized interface. In this regard, a study of the radiation effect of devices under different hole transporting materials (HTMs) is underway in order to evaluate the MAPbI_3 /HTM interface for possible oxidation under irradiation.

Conflicts of interest

There are no conflicts to declare.

Acknowledgements

The authors are thankful for financial support from Consejo Nacional de Investigaciones Científicas y Tecnológicas (CONICET, PIP 0808CO), Agencia Nacional de Promoción Científica y Tecnológica (ANPCyT, PICT 2015-1961) and Fundación Innovación y Tecnología (FUNINTEC, INTERING 2016). The authors are indebted to Martín Alurralde (DES-CNEA) for the use of the irradiation line, E. B. Halac (DMC-CNEA) for Raman measurements and to M. C. Marchi (CMA-UBA) for the SEM measurements. WOHW and NCG thank CONICET for their doctoral scholarship. MDP and PG are staff members of CONICET.

Notes and references

- 1 K. Ren, L. Huang, S. Yue, S. Lu, K. Liu, M. Azam, Z. Z. Wang, Z. Wei, S. Qu and Z. Z. Wang, *J. Mater. Chem. C*, 2017, **5**, 2504–2508.
- 2 H. Zhu, Y. Fu, F. Meng, X. Wu, Z. Gong, Q. Ding, M. V. Gustafsson, M. T. Trinh, S. Jin and X.-Y. Zhu, *Nat. Mater.*, 2015, **14**, 636–642.



3 Y. Jia, R. A. Kerner, A. J. Grede, A. N. Brigeman, B. P. Rand and N. C. Giebink, *Nano Lett.*, 2016, **16**(7), 4624–4629.

4 L. Gu, M. M. Tavakoli, D. Zhang, Q. Zhang, A. Waleed, Y. Xiao, K. Tsui, Y. Lin, L. Liao, J. Wang and Z. Fan, *Adv. Mater.*, 2016, **28**(44), 9713–9721.

5 J. P. Correa-Baena, A. Abate, M. Saliba, W. Tress, T. Jesper Jacobsson, M. Grätzel and A. Hagfeldt, *Energy Environ. Sci.*, 2017, **10**, 710–727.

6 T. Duong, J. Peng, D. Walter, J. Xiang, H. Shen, D. Chugh, M. N. Lockrey, D. Zhong, J. Li, K. J. Weber, T. P. White and K. R. Catchpole, *ACS Energy Lett.*, 2018, **3**(10), 2441–2448.

7 G. P. Nagabhushana, R. Shivaramaiah and A. Navrotsky, *Proc. Natl. Acad. Sci. U. S. A.*, 2016, **113**, 7717–7721.

8 N. J. Jeon, J. H. Noh, Y. C. Kim, W. S. Yang, S. Ryu and S. Il. Seok, *Nat. Mater.*, 2014, **13**, 897–903.

9 J. Bisquert and E. J. Juarez-perez, *J. Phys. Chem. Lett.*, 2019, **10**, 5889–5891.

10 W. Peng, C. Aranda, O. M. Bakr, G. Garcia-Belmonte, J. Bisquert and A. Guerrero, *ACS Energy Lett.*, 2018, **3**(7), 1477–1481.

11 J. Duan, H. Xu, W. E. I. Sha, Y. Zhao, Y. Wang, X. Yang and Q. Tang, *J. Mater. Chem. A*, 2019, **7**, 21036–21068.

12 M. Alurralde, M. J. L. Tamasi, C. J. Bruno, M. G. Martínez Bogado, J. Plá, J. Fernández Vázquez, J. Durán, J. Schuff, A. A. Burlon, P. Stoliar and A. J. Kreiner, *Sol. Energy Mater. Sol. Cells*, 2004, **82**, 531–542.

13 M. Ochoa, E. Yaccuzzi, P. Espinet-González, M. Barrera, E. Barrigón, M. L. Ibarra, Y. Contreras, J. García, E. López, M. Alurralde, C. Algora, E. Godfrin, I. Rey-Stolle and J. Plá, *Sol. Energy Mater. Sol. Cells*, 2017, **159**, 576–582.

14 D. Shi, V. Adinolfi, R. Comin, M. Yuan, E. Alarousu, A. Buin, Y. Chen, S. Hoogland, A. Rothenberger, K. Katsiev, Y. Losovoj, X. Zhang, P. A. Dowben, O. F. Mohammed, E. H. Sargent and O. M. Bakr.

15 Y. Tian and I. G. Scheblykin, *J. Phys. Chem. Lett.*, 2015, **6**, 3466–3470.

16 Y. Miyazawa, M. Ikegami, H.-W. Chen, T. Ohshima, M. Imaizumi, K. Hirose and T. Miyasaka, *iScience*, 2018, **2**, 148–155.

17 Y. Miyazawa, M. Ikegami, T. Miyasaka, T. Ohshima, M. Imaizumi and K. Hirose, 2015 IEEE 42nd Photovoltaic Spec. Conf. PVSC 2015, 2015, 4–7.

18 N. H. Nickel, F. Lang, V. V. Brus, J. Bundesmann, S. Seidel, A. Denker, S. Albrecht, G. Landi and H. C. Neitzert, in *Physics, Simulation, and Photonic Engineering of Photovoltaic Devices VII*, ed. A. Freundlich, L. Lombez and M. Sugiyama, SPIE, 2018, vol. 10527.

19 G. Litrico, N. Piluso and F. La Via, *Mater. Sci. Forum*, 2017, **897**, 303–306.

20 S. Nakashima, Y. Nakatake, Y. Ishida, T. Talkahashi and H. Okumura, *Phys. B*, 2001, **310**, 684–686.

21 R. Tanta, C. Lindberg, S. Lehmann, J. Bolinsson, M. R. Carro-temboury, K. A. Dick, T. Vosch, T. S. Jespersen and J. Nygård, *Phys. Rev. B*, 2017, **96**(16), 165433–165440.

22 A. Eckmann, A. Felten, I. Verzhbitskiy, R. Davey and C. Casiraghi, *Nano Lett.*, 2012, **12**(8), 3925–3930.

23 H. Yuan, X. Zhou, Y. Cao, Q. Bian, Z. Zhang, H. Sun, S. Li, Z. Shao and J. Hu, *npj 2D Mater. Appl.*, 2019, **3**, 12.

24 L. Q. Xie, T. Y. Zhang, L. Chen, N. Guo, Y. Wang, G. K. Liu, J. R. Wang, J. Z. Zhou, J. W. Yan, Y. X. Zhao, B. W. Mao and Z. Q. Tian, *Phys. Chem. Chem. Phys.*, 2016, **18**, 18112–18118.

25 C. Quarti, G. Grancini, E. Mosconi, P. Bruno, J. M. Ball, M. M. Lee, H. J. Snaith, A. Petrozza and F. De Angelis, *J. Phys. Chem. Lett.*, 2014, **5**, 279–284.

26 M. Ledinský, P. Löper, B. Niesen, J. Holovský, S. J. Moon, J. H. Yum, S. De Wolf, A. Feijfar and C. Ballif, *J. Phys. Chem. Lett.*, 2015, **6**, 401–406.

27 B. W. Park, S. M. Jain, X. Zhang, A. Hagfeldt, G. Boschloo and T. Edvinsson, *ACS Nano*, 2015, **9**, 2088–2101.

28 R. Gottesman, L. Gouda, B. S. Kalanoor, E. Haltzi, S. Tirosh, E. Rosh-Hodesh, Y. Tischler, A. Zaban, C. Quarti, E. Mosconi and F. De Angelis, *J. Phys. Chem. Lett.*, 2015, **6**, 2332–2338.

29 C. Aranda, C. Cristobal, L. Shooshtari, C. Li, S. Huettner and A. Guerrero, *Sustain. Energy Fuels*, 2017, **1**, 540–547.

30 P. Pistor, A. Ruiz, A. Cabot and V. Izquierdo-roca, *Nat. Publ. Gr.*, 2016, 1–8.

31 D. U. Wiechert, S. P. Grabowski and M. Simon, *Thin Solid Films*, 2005, **484**, 73–82.

32 N. Aristidou, C. Eames, I. Sanchez-Molina, X. Bu, J. Kosco, M. S. Islam and S. A. Haque, *Nat. Commun.*, 2017, **8**, 15218.

33 W. Kong, A. Rahimi-Iman, G. Bi, X. Dai and H. Wu, *J. Phys. Chem. C*, 2016, **120**(14), 7606–7611.

34 Y. Ouyang, Y. Li, P. Zhu, Q. Li, Y. Gao, J. Tong and L. Shi, *J. Mater. Chem. A*, 2019, **7**, 2275–2282.

35 L. Zhang and P. H.-L. Sit, *J. Mater. Chem. A*, 2017, **5**(19), 9042–9049.

